Calculation of cable thermal rating considering non-isothermal earth surface

Sujit Purushothaman[1], Francisco de León[2], Matthew Terracciano[2]

[1]Research Department, FM Global, 1125 Boston Providence Turnpike, Norwood, MA 02062, USA
[2]Department of Electrical and Computer Engineering, NYU Polytechnic School of Engineering, Brooklyn, NY 11201, USA
E-mail: p9sujit@gmail.com

Abstract: The study presents an algorithm to compute the heat transfer coefficient for thermal cable rating when modelling the non-isothermal earth surface with the additional wall method. The position of the fictitious images is computed analytically by recognising that the complex geometrical arrangement can be converted into a much simpler one using the Fourier transform. This allows for the estimation of the heat transfer coefficient with simple formulas. The resulting equations are very easy to implement and are entirely compatible with the standardised methods (IEC and IEEE) for rating power cables. Hundreds of finite elements simulations have been performed to validate the proposed method which yielded results with typical differences of <5% for standard installations.

1 Introduction

The life of the insulation of underground power cables is dependent on the maximum temperature attained by the cable core during operation. This temperature is a function of the current carried by the cable. The heat transfer coefficient at the soil–air interface is an important factor in the calculation of underground cable ampacity. The accurate computation of the heat transfer coefficient is convoluted because of the temperature variation at the earth's surface. However, the IEEE and IEC standards assume that the earth surface is an isotherm plane [1, 2]. Consequently, the thermal resistance external to the cable (duct or backfill) for buried cables is computed using the method of images. This method was proposed by Thomson (Lord Kelvin) earlier than 1848 for electrostatic problems [3]. It was expanded by him (in 1867) for both thermal and electrostatic problems including multiple sources and surface geometries [4]. For cable thermal rating, the image method is known as the Kennelly hypothesis [5] (1893). The technique was further explained by Neher [6] in 1949 for installations with multiple cables using the principle of superposition, and experimentally verified by Bauer and Nease in 1957 [7].

The importance of the image method is that it provides a convenient way to compute the temperature rise at any point in the soil as the sum of the temperature rise caused by the heat sources in the ground plus the temperature rise caused by their fictitious images above the ground [8]. However, the Kennelly hypothesis precludes considering the convective boundary conditions at the earth's surface. It has been demonstrated that for shallow installations the results of assuming an isothermal surface overestimate the ampacity of the cables [9–11]; see below Section 3.

The results of a comprehensive literature search revealed that modelling of non-isothermal earth surface is not widespread. Just over a handfull of publications discuss the matter; see [8–15]. Goldenberg [9] presents a closed-form solution to the heat transfer problem. Perhaps, because the final formula looks complicated (includes the evaluation of infinite series), no further studies seem to be made on this formulation. In [10], a comprehensive summary of the available analytical solutions is given; the fictitious layer method is discussed in detail. In this 'additional wall' method as called by the originator, Kutateladze [15], the earth surface is modelled by an imaginary layer of soil d metres thick computed as

$$d = \frac{1}{\rho h}[\text{m}] \qquad (1)$$

where ρ (k m/W) is the thermal resistivity of the soil and h (W/k m^2) is the heat transfer coefficient. The heat transfer coefficient is computed via an integral equation method using the maximum temperature of the soil surface [10, 12, 15]. Therefore the external thermal resistance ($T4$) computed using three different formulations follows the inequality [12]: $T4_{\text{isothermal}} > T4_{\text{Kutateladze fictitious layer}} > T4_{\text{non-isothermal}}$.

In [11], finite elements have been used to compare the results of isothermal and non-isothermal earth surface, but no model compatible with the standard methods (IEEE or IEC) was offered. In [13], a model based on a series of layers with different thermal resistivities was proposed.

The literature search also yielded that among the available commercial programs to compute cable ampacity only CYMCAP seems to offer modelling of the non-isothermal

earth surface [14]. It does it by using (1), but the application is restricted to air temperatures higher than soil temperatures and to comply with $d/L < 0.4$ (L is the burial depth of the cable closest to the earth surface) [15]. The latter restriction assures that the temperature distribution at the surface of the fictitious layer is an isothermal [15]. The constraint $d/L < 0.4$ precludes the modelling of 'very shallow installations', say $L < 0.5$ m.

The main contribution of this paper is the calculation of the heat transfer coefficient h with simple (no integrals), yet accurate formulas, applicable to the modelling of non-isothermal earth surface (including very shallow installations). By the use of the Fourier transformation, the position of the fictitious image is obtained by verifying (1). The final expressions are simple and are completely compatible with the standard methods used for cable thermal rating [1, 2]. The paper in addition to proposing a formula to calculate the heat transfer coefficient, presents the implementation of the Fourier transform to convert the two-dimensional (2D) problem into a 1D problem.

The model presented in this paper (hereafter referred to as the analytical solution) has been validated with hundreds of finite element model (FEM) simulations. There is in the literature substantial experimental verification of the IEC standard calculations for underground cables [16–18] and FEM simulations [19, 20]. Our FEM calculations match very well with those experiments. In addition, to enhance the confidence with the FEM simulations, the results of the experiments presented in [21] have been reproduced by simulation with a 0.5% difference. Other interesting simulations are presented in [22].

The results presented in this paper extend for installation depths from 0.05 to 2.5 m. The installation of high-voltage cables at very shallow depths is prohibited for safety reasons (depths < 0.5 m). However, the selected shallow installation depth of 0.05 m is considered in the paper for its theoretical value. The deeper installation limit of 2.5 m is chosen, in addition to its academic value, because for the short distances for avoiding the obstacles (e.g. crossing roads, railroads, other cables and other obstructions) this depth is possible. Moreover, the deeper section along the run of the cable is frequently the bottle neck and therefore it determines the ampacity of the circuit. Without loss of generality the simple cable construction given in the Appendix has been selected for the study. The paper focus is on the effects of the non-isothermal earth surface on the temperature rise of cables. In terms of the IEC Standards, the paper only

deals with $T4$ (the external to the cable thermal resistance), but all internal layers can be represented when required following the IEC standards.

2 Theoretical considerations

2.1 Fourier transform

The application of Fourier transform to the complex geometry of directly buried cables, significantly simplifies the analysis of the problem. Specifically, the 2D heat transfer problem of a directly buried cable is converted into a 1D problem by the application of the Fourier transform. The following equation describes the process

$$\mathbb{F}\{T(x, y)\} = \overline{T}(s, y) \tag{2}$$

where x and y are the horizontal and vertical coordinates, respectively, and s corresponds to horizontal components in the transformed (Fourier) domain.

Fig. 1a shows a cable with Q_s (W/m) losses directly buried in the soil of thermal resistivity ρ. The cable is placed at a burial depth L (m) from the surface exposed to an ambient air temperature T_{air}. A cable can be considered as a point source when compared with the vast expanse of the soil region. Hence, the heat source could be expressed as a Dirac-delta function $\delta(x)$ at depth L from the surface, where the heat flux is Q_s only at the position of the cable and zero elsewhere. Fourier transform theory states that

$$\mathbb{F}\{\delta(x)\} = 1 \tag{3}$$

This indicates that a cable in the space domain can be represented by a straight line with constant heat flux in the Fourier domain as shown in Fig. 1.

Owing to the 2D nature of the original problem, the temperature at the surface, $T_{surface}$ is a function of x, with the maximum temperature directly above the cable ($x = 0$) and gradually decreasing as one moves away (more on this can be found below in Section 3). This significantly convolutes the evaluation of the heat transfer coefficient h (x) for the soil surface (in the spatial domain). The Fourier domain of Fig. 1b presents a simplified geometry. The cable becomes a constant line source and the temperature at the soil surface $\overline{T}_{surface}$ is constant. $\overline{T}_{surface}$ can be computed iteratively to satisfy the heat equation at the soil surface $\overline{T}_{surface} = T_\infty + Q_s/\overline{h}$, convergence of which is obtained in a few iterations. Thus, the calculation of the heat transfer
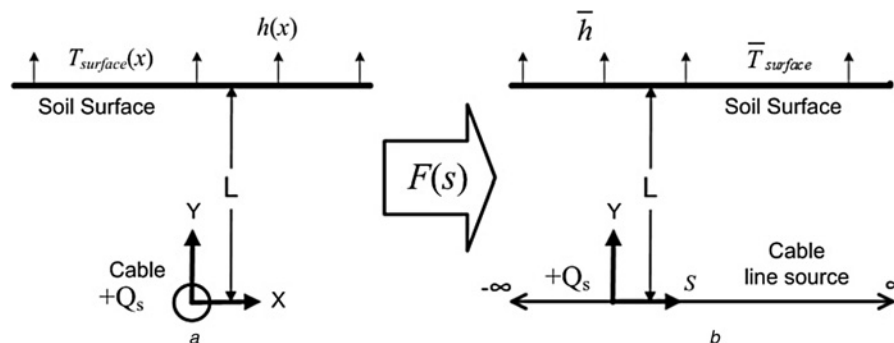
Fig. 1 *Directly buried cable transformed to the Fourier domain*
a Geometry in spatial domain
b Geometry in Fourier domain

coefficient, $\overline{h}$ (in the transformed domain) is simplified and can be obtained as follows [23–25]

$$\overline{h} = Nu \, k/L_c \tag{4}$$

where k is the thermal conductivity of air, L_c is the characteristic length (the ratio of surface area to perimeter) of the soil surface. For an infinite soil surface $L_c = 0.5$, and Nu is the Nusselt number given by

$$Nu = C \, Ra_{Lc}^m \tag{5}$$

Equation (5) is valid for heat transfer because of laminar flow of fluid, which in our case is air. The different values of C and m are due to piece-wise approximation of the Nusselt number in the laminar flow domain. The validity of this equation has been experimentally verified in [23]. The values of C and m are given in Table 1 ([23, 24]). The Rayleigh number Ra_{Lc} is computed from

$$Ra_{Lc} = Gr_{Lc} Pr \tag{6}$$

where Gr_{Lc} is the Grashof number and Pr is the Prandtl number given by

$$Gr_{Lc} = \frac{g\beta(\overline{T}_s - T_\infty)L_c^3}{\nu^2} \tag{7}$$

and

$$Pr = \frac{C_p\mu}{k} \simeq 0.7 \text{ (for air)} \tag{8}$$

where g is the acceleration due to gravity ($= 9.8$ m/s^2); β is the volumetric thermal expansion coefficient $[1/K] = 1/T_s$; $\mu = $ dynamic viscosity$[Pa \cdot s] = 1.827 \times 10^{-5}\left(\frac{410.85}{\overline{T}_s + 120}\right)\left(\frac{\overline{T}_s}{291.15}\right)^{1.5}$; C_p is the specific heat capacity at constant pressure $= 1006$ J/kg K; ν is the kinematic viscosity [m^2/s] $= \mu/\alpha$; α is the air density [kg/m^3] $= 352.98/T_s$; $k = 1.5207 \times 10^{-11}\overline{T}_s^3 - 4.857 \times 10^{-8}\overline{T}_s^2 + 1.0184 \times 10^{-4}\overline{T}_s - 3.9333\times 10^{-4}$; $\overline{T}_s = (\overline{T}_{surface} + T_\infty)/2 = $ average surface-ambient temperature (K); $T_\infty = $ ambient air temperature (K).

It is of paramount importance to note that the value of $\overline{h}$ using (4) to (8) is independent of cable depth and cable dimensions. The heat transfer coefficient in the transformed domain depends only on the physical properties (of air) and the amount of heat dissipated.

2.2 Solution of the transformed domain problem

After the application of the Fourier transform, the 2D heat transfer problem reduces to the solution of the 1D diffusion

Table 1 Calculation of Nusselt number from the Rayleigh number [23]

Range Ra$_L$	C	m
1–200	0.96	1/6
200–8 × 10^6	0.54	1/4
8 × 10^6–3 × 10^{10}	0.14	1/3

equation [24] as follows

$$\frac{d^2}{dy^2}\overline{T}(s, y) = 0 \tag{9}$$

subjected to the following boundary conditions

$$-k\frac{d\overline{T}(s, y)}{dy}\bigg|_{y=L} = h \times \overline{T}(s, y = L) \tag{10}$$

$$-k\frac{d\overline{T}(s, y)}{dy}\bigg|_{y=0} = \overline{Q}_s \tag{11}$$

The solution of (9) with (10) and (11) yields

$$\overline{T}(s, y) = -\overline{Q}_s\rho y + \frac{\overline{Q}_s}{\overline{h}}\left(1 + \overline{h}\rho L\right) \tag{12}$$

The thermal problem of Fig. 1a can also be analysed with the method of images; see Fig. 2a. The Fourier transform applied to this geometry produces that the cable (heat source) and the image (heat sink) become a line source and a sink, respectively; see Fig. 2b. The non-isothermal earth surface can be modelled with the help of a fictitious earth layer with thickness d [15]. The cable image line source (sink) is placed at distance $L' = L + d$ above the fictitious layer.

The governing equation is the same as (9). The boundary condition (11) is applicable because of the same line source. In addition, at $y = 2L'$ we have

$$-k\frac{\partial d(s, y)}{dy}\bigg|_{y=2L'} = -\overline{Q}_s \tag{13}$$

Owing to a uniform temperature gradient, one can see that

$$\overline{T}(s, y)\big|_{y=L'} = 0 \tag{14}$$

Substituting (14) and (11) in (9), we obtain

$$\overline{T}(s, y) = -\overline{Q}_s\rho y + \overline{Q}_s\rho L' \tag{15}$$

Comparing (12) and (15) we see that

$$d = \frac{1}{\overline{h}\rho} \tag{16}$$

As stated earlier, this equation has been proved long back [10, 12] in the spatial domain. However, the real challenge in the applicability of (1) is the evaluation of h since the surface temperature is not constant. The difficulty is overcome in this paper by solving the problem in the Fourier domain where the evaluation of $\overline{h}$ is relatively simple with (4)–(8). We make the important remark that since $\overline{h}$ is only used here to compute the thickness of the fictitious layer, there is no need to take the inverse Fourier transform. This means that the dependency of the fictitious layer on cable dimensions and installation depth is completely eliminated. The validity range of (4) and (16) will be established numerically in the next section using finite element simulations.

The algorithm to calculate the heat transfer coefficient is an iterative process and is detailed in Fig. 3.
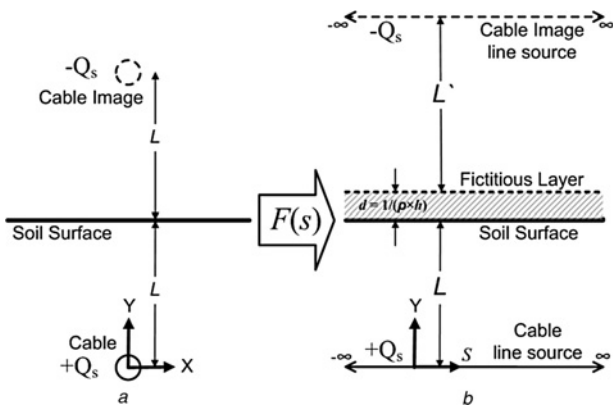
Fig. 2 *Method of images transformed to the Fourier domain;*
a Cable and its image in spatial domain;
b Cable and its image in Fourier domain
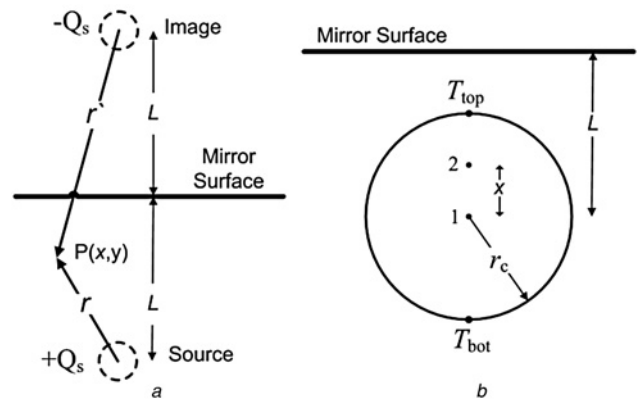
Fig. 4 *Point source correction for cables directly buried in soil*
a Solution of image problem;
b Eccentricity correction
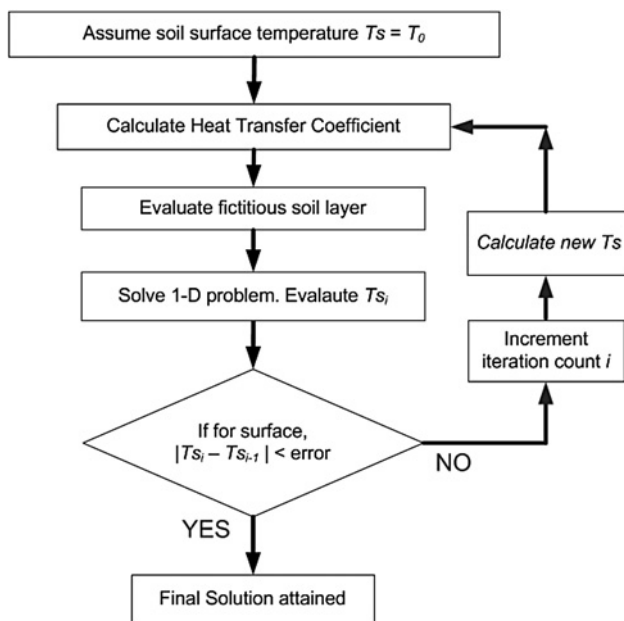
Fig. 3 *Algorithm for calculating the heat transfer coefficient*

2.3 Point source correction

The solution of the image problem described in Fig. 3 is [3]

$$T_p(x, y) = T_{\text{amb}} + \frac{\rho Q_s}{2\pi} \ln\left(\frac{r'}{r}\right) \qquad (17)$$

where $T_p(x, y)$ is the temperature at point P with coordinates x and y and T_{amb} is the ambient soil temperature.

The solution assumes that the heat sources are filamentary. However, in reality the entire cable core acts as the heat source. This along with the proximity to the non-isothermal earth surface can drastically deform the isotherms around the cable; see Section 3. Also since the cable core is made of high thermal conductivity material, the entire circular region with radius r_c is isothermal. To equate this physical reality to the point source problem, the point source must be relocated from point 1 (geometric centre of the cable) to point 2 (corrected location) as shown in Fig. 4.

The heat source location is corrected by distance x such that the cable core surface is an isotherm. By using (17) to evaluate and equate the top and bottom temperatures of the cable core, T_{top} and T_{bot}, we obtain

$$x = L - \sqrt{L^2 - r_c^2} \qquad (18)$$

It has been observed that the point source correction yields about 1% improvement on the results when the correction is not used and is more significant for shallow installations.

3 FEM simulations and validation

To establish the validity range of the formulas given in the IEC standard and the model given in the above section, hundreds of FEM simulations were performed. The maximum temperature attained by a single (or set of cables) directly buried in soil is used as the measurement parameter. In conjunction with simulations, the accuracy of the image method in determining these values was tested.

3.1 Convective cooling against fixed temperature boundary

According to the IEC and IEEE standards, cable ampacity is computed assuming that the earth surface is an isotherm plane [1, 2]. This leads, potentially, to large errors in the calculated conductor temperature against actual temperature because heat transfer to and from the external air is not taken into account. To find the errors of assuming an isothermal earth surface, hundreds of finite elements (FEM) simulations are performed. All finite element simulations of this paper were performed using the heat transfer module of COMSOL Multiphysics [26], which allows for the representation of problems involving conduction, convection and radiation. Simulations using several methods are compared: (i) an isotherm surface with FEM; (ii) image method with FEM; (iii) IEC formulas; and (iv) a convective cooling boundary along the soil boundary. All the cases were run with constant cable loss in the steady state to obtain the graph in Fig. 5. The FEM model has 9664 elements of second order. The solver used is a stationary fully coupled solver. The geometry used is 20 m wide by 7 m deep. The lower boundary is an infinite element boundary to simulate the infinite soil domain. The vertical boundaries are set as Neumann boundaries. The soil surface (top boundary) is set as a convective boundary. The convective cooling boundary condition effectively simulates the effects because of
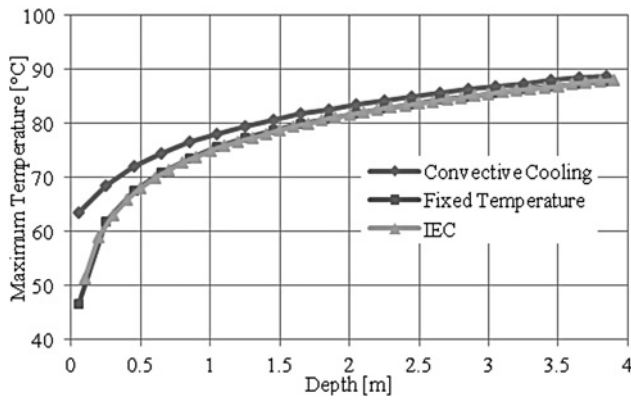
Fig. 5 *Maximum temperature attained against depth of cable for 50 W/m dissipation with equal soil and ambient temperature of 10°C and soil resistivity of 1.2 m K/W*

convection to ambient air above the surface without the need to simulate the complicated natural convection associated with the phenomenon.

Only three curves are shown in Fig. 5 because the results of the image method with the FEM and the IEC methods are identical. Also, one can observe that the temperatures computed with the IEC method and the FEM simulations with fixed boundary temperature at the surface are very close to each other. However, there is a significant difference in conductor temperature when the results are compared with the more realistic convective cooling boundary condition. The temperature difference found, for shallow cable installations (0.5 m), between the standard fixed temperature boundary and the more accurate convective cooling boundary condition at the soil–air layer is around 6.5%. The error is larger for very shallow installations. As expected, the differences become smaller as the depth of the installation increases. At the typical installation depths (1 m) the difference is about 4%.

Figs. 6a and b present a typical 3 × 3 cable installation of buried cables used to show the differences between convective cooling and fixed boundary. It can be noted by observing Fig. 6a that when a fixed temperature boundary is used the isotherm lines associated with the temperature distribution in the soil do not intersect the soil–air boundary, illustrating an unrealistic model of the physical phenomenon. However, when a convective cooling boundary is applied, as seen in Fig. 6b, the isothermal lines intersect the soil–air boundary and show a large variation of the temperature along the soil surface, representing more realistically the temperature distribution seen at the soil surface.

3.2 Verification of isotherms for the image method

As described in Section 2, the image method can be modified to account for a convective cooling boundary (non-isothermal) condition at the soil–air boundary. To verify that the proposed (4) and (16) are accurate for realistic cases, the maximum temperature achieved in the conductor as well as the isothermal lines showing the temperature distribution within the soil must match those found with the convective cooling case. This will ensure that the variables h and d calculated numerically with FEM simulations match with those found analytically in Section 2.
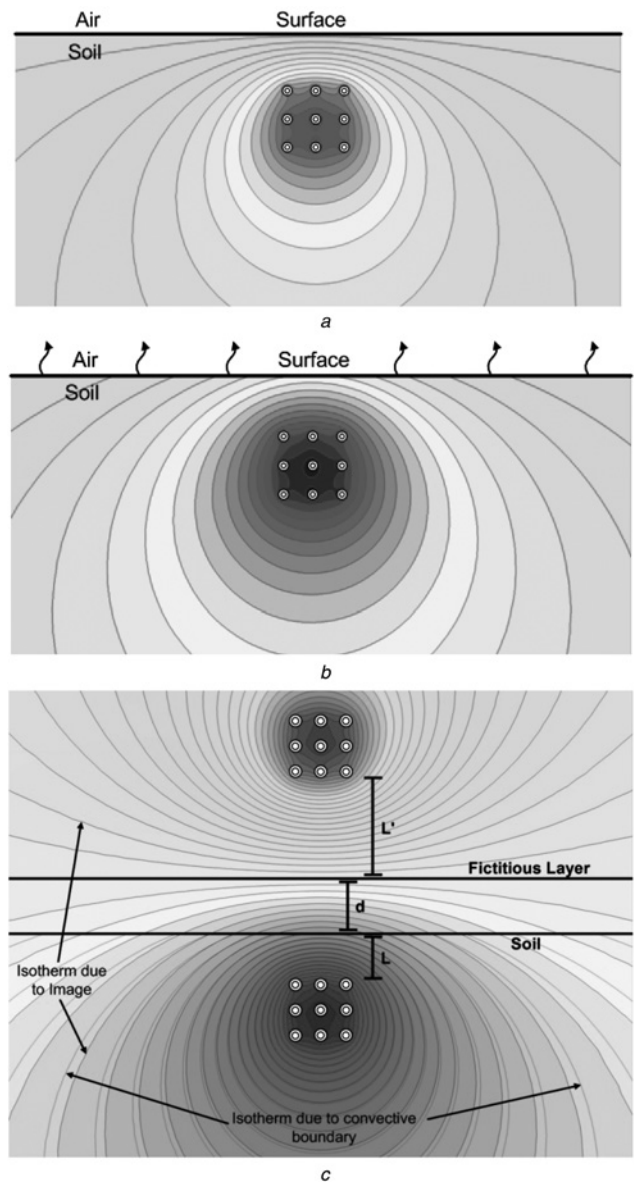
Fig. 6 *Isotherms for a typical 3 × 3 cable installation of buried cables*

a Assuming a fixed temperature boundary at the surface
b Assuming a convective cooling boundary at the surface
c Convective cooling and image method

As seen in Fig. 6c, the isotherms associated with a convective cooling boundary at the soil, shown outlining the colour gradient, mimic those obtained when using the image method. These results give great confidence in the accuracy of the image method to replicate the results found with the convective cooling boundary condition when the air temperature equals the ambient temperature of the soil. Note that the soil and fictitious layer lines in Fig. 6c are straight and parallel, but there is an optical illusion caused by the curvature of the isotherms.

3.3 Comparison with FEM

The validity of the proposed theory for realistic cable installations is very important. The results of the formulation of this paper are compared with hundreds of FEM simulations. A range of parametric tests are performed on single, trefoil, flat and 3 × 3 cable formations varying soil

resistivity and depth of cable installation. It must be noted that the method is independent of cable construction and is completely general. The cable used in this study is similar to the one used in [27]. The details of the cable are given in the Appendix. Results for each installation are presented for 8 values of ρ at 16 values of cable depth. These 128 cases are compared against the proposed model for each installation which sums up to a total of 512 simulations. All simulations are run for an ambient temperature of 20°C. Fig. 7a–d plot the percent difference whereas Tables 2–4 present the best and worst match of the maximum cable core temperature (any of the parallel cables) with FEM simulations.

Results are obtained for a single cable installation with the cable depth (L) varied from 0.05 to 2.5 m (for theoretical completeness) for soil resistivity (ρ) variation from a minimum of 0.3 m K/W to a maximum of 4 m K/W. The best and worst results are presented in Table 2. Fig. 7a presents the percent difference for a total of 128 cases. The method gives an almost perfect match for standard cable depths and higher soil resistivities at shallow depths.

A parametric variation of ρ and L is performed for trefoil installations. Table 3 shows a maximum of 2.6% difference for standard depths. Fig. 7b depicts how the error amplifies for shallow depths, details of which are discussed in the later part of this section.

A flat cable formation with a separation of one cable diameter is used for parametric sweep of ρ and L. Table 4 shows a maximum of 1.79% difference for standard cable depths. Fig. 7c shows an acceptable difference range (−2 to 2%) for standard depths. The cumulative results are similar to those of the trefoils but with enlarged differences for shallow installations.

A 3×3 cable formation with a separation of one cable diameter is used for parametric sweep of ρ and L. Table 5 shows a maximum of 5.5% difference for standard cable depths. Fig. 7d shows the error to vary between −3 and 6.5% for standard depths. Contrary to previous installation types, the differences reduce for shallow 3×3 installations.

Even though the theory was developed for a single heat source, the method was successfully implemented for multiple heat sources (trefoil, flat formations and 3×3 arrangements). It has been demonstrated that the model works effectively for these practical installations and provides confidence in the proposed method.

The problem of considering multiple heat sources is solved using superposition. This is applicable strictly to a linear problem. However, the problem at hand is made non-linear because of the nature of h. In addition, since the flat and 3×3 installations consist of heat sources separated by a distance, the deviation from a point source geometry is larger and hence can be a contributing factor to the slightly larger differences.

Even though very shallow installations are not practical for safety reasons, the results were presented for theoretical completeness. Fourier analysis assumes that the heat sources (cables) are filamentary. However, for very shallow installations, this is not the case since the dimensions of the cables are comparable with the depth. Hence, the model yields larger differences for shallow depths.

Fig. 8 plots the temperature variation along the soil surface for various cable installation depths obtained with FEM simulations. It is observed that for very shallow installations, that is, cables installed <0.5 m from the surface, the temperature varies significantly. In addition,
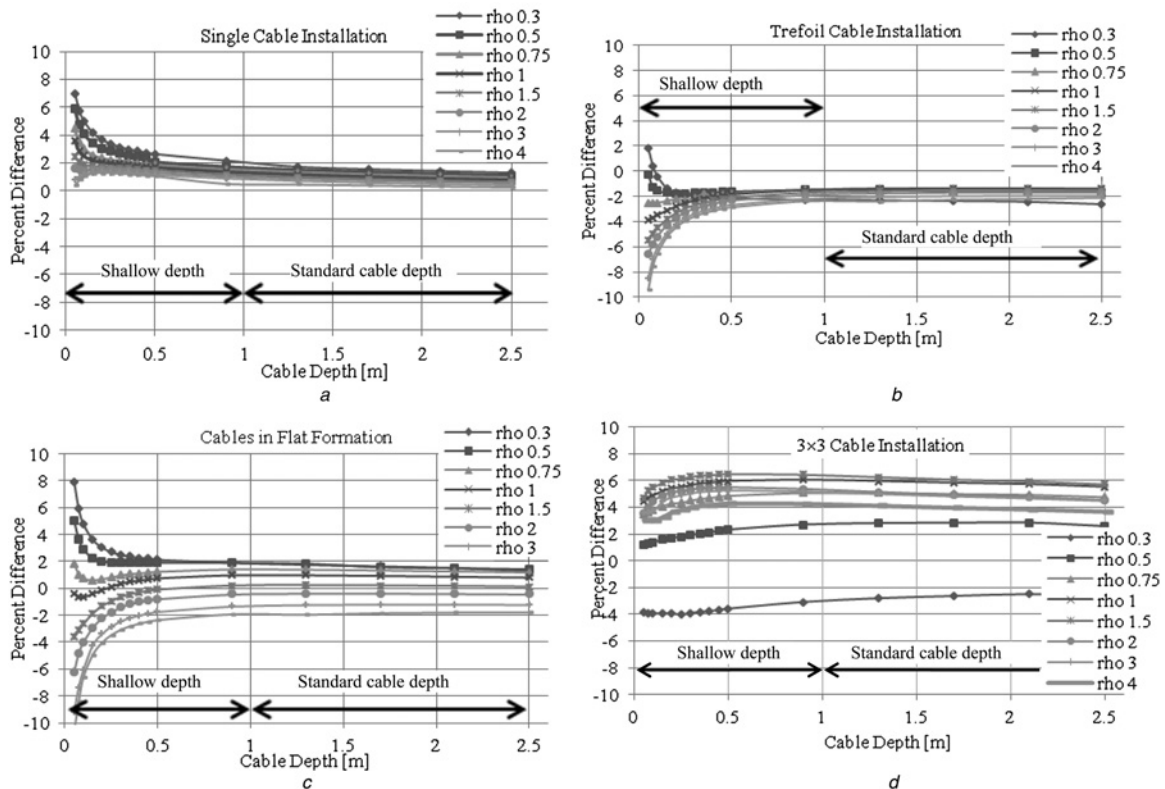
Fig. 7 *Percent difference against cable depth for various soil resistivities*

a Single cable installation
b Trefoil cable installation
c Cables in flat formation
d 3×3 Cable installation

Table 2 Comparison between FEM and analytical method for single cable installation (ambient temperature $T_s = 20°C$)

ρ, m K/W	L, m	Q, W/m	Temperature,°C FEM	Temperature, °C Analytical	% difference	
					$T_{absolute}$	ΔT
0.3	0.05	123.49	85.89	79.93	6.94	9.05
0.3	2.5	123.49	90.00	88.84	1.28	1.66
1	0.05	61.5	69.22	66.72	3.62	5.08
1	2.5	61.5	90.00	89.29	0.79	1.01
4	0.05	19.6	51.22	51.03	0.37	0.61
4	2.5	19.6	89.97	89.74	0.26	0.33

Table 3 Comparison between FEM and analytical method for trefoil cable installation (ambient temperature $T_s = 20°C$)

ρ, m K/W	L, m	Q, W/m	Temperature, °C FEM	Temperature, °C Analytical	% difference	
					$T_{absolute}$	ΔT
0.3	0.05	65.03	81.27	79.76	1.86	2.46
0.3	2.5	65.03	89.99	92.36	−2.64	−3.39
1	0.05	26.62	63.16	65.62	−3.89	−5.70
1	2.5	26.62	90.00	91.25	−1.39	−1.79
4	0.05	7.69	48.45	53.02	−9.45	−16.06
4	2.5	7.69	89.92	91.84	−2.13	−2.75

Table 4 Comparison between FEM and analytical method for flat cable installation (ambient temperature $T_s = 20°C$)

ρ, m K/W	L, m	Q, W/m	Temperature, °C FEM	Temperature, °C Analytical	% difference	
					$T_{absolute}$	ΔT
0.3	0.05	66.51	82.03	75.53	7.93	10.48
0.3	2.5	66.51	90.00	88.84	1.28	1.66
1	0.05	26.7	61.90	62.13	−0.37	−0.55
1	2.5	26.7	89.98	89.25	0.81	1.04
4	0.05	7.75	43.99	48.69	−10.69	−19.59
4	2.5	7.75	89.95	91.57	−1.79	−2.32

Table 5 Comparison between FEM and analytical method for 3×3 cable installation (ambient temperature $T_s = 20°C$)

ρ, m K/W	L, m	Q, W/m	Temperature, °C FEM	Temperature, °C Analytical	% difference	
					$T_{absolute}$	ΔT
0.3	0.05	33.11	72.68	75.47	−3.83	−5.30
0.3	2.5	33.11	89.98	92.26	−2.54	−3.26
1	0.05	10.84	61.22	58.52	4.41	6.55
1	2.5	10.84	89.99	85.04	5.50	7.07
4	0.05	3	50.42	48.91	3.01	4.96
4	2.5	3	89.87	86.60	3.64	4.68
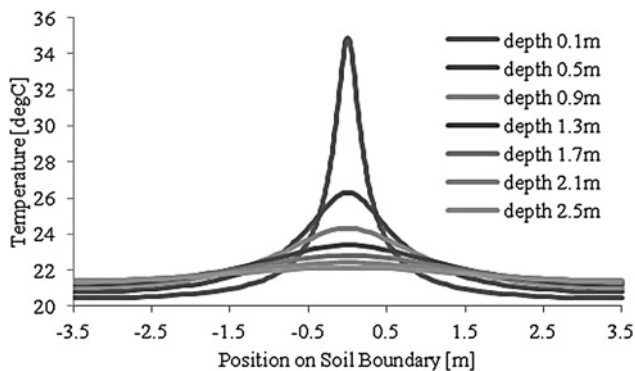
Fig. 8 *Soil surface-temperature variation for various cable depths; $\rho_{soil} = 2.0$ m K/W, $T_{amb} = 20°C$, $Q_{loss} = 36$ W/m*

because of the higher temperature difference between the soil surface and ambient air in shallow installations, heat transfer by radiation is also significant. These are the reasons for increased differences in Tables 2–4 for very shallow installations. Note, however, that very shallow installation of high-voltage cables (under 0.5 m) may be dangerous and it is prohibited in most places. Furthermore, even for shallow installations the methods proposed in this paper give acceptable results for the thermal rating of cables.

4 Conclusions

An integral transformation (Fourier transform) was applied to convert the complicated 2D heat transfer problem of directly

buried cables to a simple 1D problem. The position of the images has been obtained analytically by recognising that there is no need to compute the inverse transformation when one is only looking for the location of the images. A simple, yet accurate, procedure has been proposed for the calculation of the heat transfer coefficient for the modelling of the non-isothermal earth surface. This is possible because in the Fourier domain the heat transfer coefficient becomes only a function of the physical properties of air and heat dissipated by the cable. It is independent of soil resistivity, cable dimensions and installation depth.

The method has been implemented successfully for common installations and is fully compatible with the standardised methods (IEC and IEEE) for rating power cables. With hundreds of finite elements simulations, the validity range of the method has been established.

Utilising FEM software to model underground cables is time-consuming and computationally intensive. The paper proposes a computationally efficient and easy to implement algorithm than can help to accurately calculate cable ampacity considering non-isothermal soil. The algorithm is compatible with the IEC Standard calculation methods and therefore any cable construction can be modelled.

5   References

1   Electric Cables – Calculation of the current rating – Part 2: Thermal resistance – Section 1: Calculation of the thermal resistance. IEC Standard 60287-2-1 (2001–11)
2   IEEE Standard Power Cable Ampacity Tables, IEEE Std. 835–1994
3   Thomson, W. (Lord Kelvin): 'Theory of electricity', *Camb. Dublin Math. J.*, 1848, **III**, p. 131
4   Thomson, W. (Lord Kelvin), Tait, P.G.: 'Natural philosophy' (Oxford at the Clarendon Press, 1867)
5   Kennelly, A.E.: 'On the carrying capacity of electric cables submerged, buried and suspended in air'. Minutes of the Ninth Annual Meeting, New York, N.Y., 1893
6   Neher, J.H.: 'The temperature rise of buried cables and pipes', *AIEE Trans.*, 1949, **68**, (1), pp. 9–21
7   Bauer, C.A., Nease, R.J.: 'A study of the superposition of heat fields and the Kennelly formula as applied to underground cable systems', *AIEE Trans. Power Deliv. III*, 1957, **76**, (3), pp. 1330–1337
8   Anders, G.: 'Rating of electric power cables: ampacity computations for transmission, distribution, and industrial applications' (IEEE Press, 1997)
9   Goldenberg, H.: 'Transient temperature rise to a line source in a semi-infinite medium, with a radiation boundary condition at the interface', *Br. J. Appl. Phys.*, 1959, **10**, pp. 314–317
10 King, S.Y., Aust, F.I.E., Foo, P.Y., Halfter, N.A.: 'External thermal resistances of shallow buried cables', *Inst. Eng. Aust. Electr. Eng. Trans.*, 1975, **11**, (2), pp. 44–49
11 Swaffield, D.J., Lewin, P.L., Sutton, S.J.: 'Methods for rating directly buried high voltage cable circuits', *IET Gener. Transm. Distrib.*, 2008, **2**, (3), pp. 393–401
12 King, S.Y., Halfter, N.A.: 'Underground power cables' (Longman Group Limited, Burnt Mill, Harlow, Essex, UK, 1982)
13 Lewin, P.L., Theed, J.E., Davies, A.E., Larsen, S.T.: 'Method for rating power cables buried in surface troughs', *IEE Proc. Gener. Transm. Distrib.*, 1999, **146**, (4), pp. 360–364
14 CYMCAP Users' Guide version 5.04, CYME International T&D Inc. St-Bruno, Quebec, 2010
15 Kutateladze, S.S.: 'Fundamentals of heat transfer' (Academic Press Inc., New York, 1963) Translated from Russian: 'Osnovy Teploobmena', Mashgiz, Moscow-Leningrad, 1962
16 Neher, J.H., McGrath, M.H.: 'The calculation of the temperature rise and load capability of cable systems', *AIEE Trans. III, Power Appar. Syst.*, 1957, **76**, pp. 752–772
17 Neher, J.H.: 'The transient temperature rise of buried cable systems', *IEEE Trans. Power Appar. Syst.*, 1964, **PAS-83**, pp. 102–114
18 Stangl, J.: 'Increased loading of distribution feeder cables at B.C. Hydro'. April 1997
19 Canadian Electrical Association: 'Ampacity calculation on power cables & cyclic loading for distribution cables in Duck Bank – Volume I: overview of the technical and experimental developments'. Contract No. 138-D-375 and No. 137-D-374, October 1986
20 Phillips Cables: 'FIECAG ampacity program – evaluation phase I'. Engineering Report No. 87–30, December 1987
21 Yong-Chun, L.: 'Steady-state thermal analysis of power cable systems in ducts using streamline-upwind/Petrov-Galerkin finite element method', *IEEE Trans. Dielectr. Electr. Insul.*, 2012, **19**, (1), pp. 283–290
22 Mazzanti, G.: 'The combination of electrothermal stress, load cycling and thermal transients and its effects on the life of high voltage ac cables', *IEEE Trans. Dielectr. Electr. Insul.*, 2009, **16**, (4), pp. 1168–1179
23 Martynenko, O.G., Khramtsov, P.P.: 'Free convective heat transfer' (Springer-Verlag, Berlin Heidelberg, 2005)
24 Bird, R.B., Stewart, W.E., Lightfoot, E.N.: 'Transport phenomena' (John Wiley and Sons. Inc., 2007, 2nd edn.)
25 Kakac, S., Yener, Y.: 'Convective heat transfer' (CRC Press, 1995, 2nd edn.)
26 Comsol Multiphysics, Heat Transfer Module User's Guide, Comsol AB Group, 2006, pp. 1–222
27 Terracciano, M., Purushothaman, S., DE León, F., Farahani, A.: 'Thermal analysis of cables in unfilled troughs: investigation of the IEC standard and a methodical approach for cable rating', *IEEE Trans. Power Deliv.*, 2012, **27**, (3), pp. 1423–1431

6   Appendix – Cable data

Owing to its simple construction, the characteristics of a 500 MCM welding cable was used in this paper (similar to one used in [27]); details as follows:

- Diameter of stranded copper conductor: 17.93 mm;
- Unfilled XLPE insulation thickness: 11 mm.